university of groningen / faculty of science and engineering

Physics Bachelor Research Project

Improving the Signal Readout of an eEDM Experiment

Author:
Vedang Kaustubh Sumbre
(S4411714)

First Supervisor:
Dr. L. Willmann
Second Supervisor:
Prof. Dr. J. Even

July 11, 2023

Abstract

The NL-eEDM experiment aims to determine a new upper limit for the electron electric dipole moment, using a molecular BaF beam. The experiment uses the $F = 0$ and $F = 1$ hyperfine levels of the ground state. The molecules in one state are depleted using laser induced fluorescence. This produces the signal readout which shows two peaks corresponding to the two levels, with a frequency difference $\omega_{HFS} = 46.86$MHz between them. This thesis explores the use of acousto-optical modulators to improve the signal readout of the experiment by probing both hyperfine levels at once. First, a method is developed to model the molecular depletion with different laser intensity distributions and detuning. A 200MHz and a 40MHz AOM are used and compared, and the 40MHz AOM is chosen for implementation into the experiment, as the output beams have good spatial separation and power outputs.

Contents

1 Introduction

This thesis has been performed in the context of the ongoing NL-eEDM experiment, which aims to provide an improved limit on the permanent electric dipole moment of the electron [1].

The Standard Model (SM) of particle physics was developed as a theory to classify known fundamental subatomic particles, and describe their interactions via the fundamental forces: strong, weak, and electromagnetic. Within the SM, the electron is a negatively charged lepton with spin-1/2. The electron has an angular momentum due to its spin and its orbital motion. This produces a magnetic dipole, and hence a magnetic dipole moment which has a non-zero value. Since there is a non-zero magnetic dipole moment, there is also the possibility of an electric dipole moment. However, the presence of a non-zero value of the electron electric dipole moment (eEDM) violates both parity ($\mathcal{P}$) and time reversal ($\mathcal{T}$) symmetries. At first, the violation of $\mathcal{P}$ symmetry was believed to be impossible based on theoretical symmetry arguments [2], but there was no argument as to why $\mathcal{P}$ was a symmetry that had to be obeyed. Lee and Yang [3] and C.S. Wu [4] experimentally proved that $\mathcal{P}$ symmetries are violated in weak interactions, and so searches for permanent dipole moments of fundamental particles continued, as proposed by Purcell and Ramsey in 1950 [2], who proposed an experimental test for an EDM to investigate $\mathcal{P}$ violation.

An EDM measurement can be performed using the structure of the Hamiltonian $\mathcal{H}$ of an electron [5]:

$$\mathcal{H} = (-\vec{\mu_e} \cdot \vec{B} - \vec{d_e} \cdot \vec{E_{eff}})\vec{S} \tag{1}$$

Where $\vec{\mu_e}$ and $\vec{d_e}$ and are the magnetic and electric dipole moments of the electron, $\vec{B}$ is the magnetic field, $\vec{S}$ is the spin of system, and $\vec{E_{eff}}$ is the effective electric field experienced by the electron. This electric field is the applied electric field that is then amplified due to the structure of the molecule, allowing for more sensitive measurements even with smaller field strengths. The energy eigenstates can be measured in a way such that there is a measurable energy difference $\delta = 2 * \vec{d_e} * \vec{E_{eff}}$ [1].

The most recent theoretical upper bound for the equivalent electron EDM in the standard model is $d_e = 1.0 \cdot 10^{-35} e$ cm [6]. While this value is several orders of magnitude lower than current experimental capacity, there are extensions of the standard model (theories that aim to fill in the gaps in the standard model) where the EDM value is lower [7], such as supersymmetry (SUSY). Several experiments are being done around the world using different experimental techniques to determine new bounds. The current upper bound was set as $|d_e| < 4.1 \cdot 10^{-30} e$ cm at 90% confidence using trapped HfF^+ ions [8]. It was set at $|d_e| < 1.1 \cdot 10^{-29} e$ cm at 90% confidence using a beam of ThO [9]. Using YbF, the lower bound was set at $10.5 \cdot 10^{-28} e$ cm at 90% confidence [10]. Perspectives on electric dipole moment searches and experiments, along with a summary of current experimental results, can be found in [11].

The value of the electron EDM is orders of magnitude smaller in the SM than it is in several SM extensions. This, along with the $\mathcal{P}$ and $\mathcal{T}$ violations, make the measurement of the EDM a good test for new physics [5], and could allow for a better understanding of matter-antimatter asymmetry in the universe [7], depending on the value of d_e.

1.1 The NL-eEDM Experiment

The NL-eEDM experiment has been set up with the aim to measure an eEDM sensitivity of $5 \cdot 10^{-30} e$ cm using a Stark decelerated cold beam of barium monofluoride (BaF) [1]. BaF is chosen as a viable candidate due to its valence electron being exposed to a large internal electric field, which enhances the eEDM and creates a linear measurable Stark shift. Although BaF has a smaller E_{eff} than other suitable molecules, it is lighter than them, allowing for it to be decelerated. BaF also has an electronic ground state structure that can be used for both laser cooling and LIF, making it a good candidate.

The set up uses the ground state of the BaF molecules, which splits into the $F = 0$ and $F = 1$ hyperfine levels. The molecules are optically pumped from the $F = 0$ level to the $F = 1$ level to create a superposition between the $m_f = 1$ and $m_f = -1$ sub-levels, which leads to a measurable phase difference ϕ.

The BaF molecules used are produced with a supersonic laser ablation beam source [12] at section A in Figure 1. This produces pulses of molecules of central velocity $v = 600$m/s, with approximately 6×10^8 molecules per steradian per pulse in the $v = 0$, $N = 1$ state [13].

At section B1, the total number of molecules in the $X^2\Sigma_{1/2}$, $N = 1$ state is probed using LIF before the molecules enter the interaction zone. This signal probing allows for the normalization of the signal after the interaction zone. Details on the normalization procedure can be found in [14], [15].
When the molecules are produced, they are thermally distributed over all molecular states, so the $F = 0$ and $F = 1$ states have approximately the same number of molecules. In section B, the molecules in $F = 1$ are brought to the $F = 0$ state, using optical pumping to the $A^2\Pi_{3/2}$ excited state. The population of the $N = 0$ ground state is largely prepared in the $|0, 0\rangle$ state [15].

After the production and optical pumping, the molecules enter the interaction zone, region C, where the spin-precession [16] takes place. A detailed discussion of the interaction zone can be found in [14].

A two photon transition is used to create the superposition between states, which are created using two coherent laser beams that enter the set-up at D2 and propagate towards the molecular beam. Details on the two photon pulses can be found in [13], [15].

The BaF molecules cannot be counted directly, so they are counted using laser-induced fluorescence (LIF) at D1 (also at B1). The molecules are excited to the $A^2\Pi_{3/2}$ state using a near infrared laser beam [17]. Depending on the laser frequency, this will lead to the molecules in either hyperfine level emitting a photon, which is then counted using a photomultiplier tube.

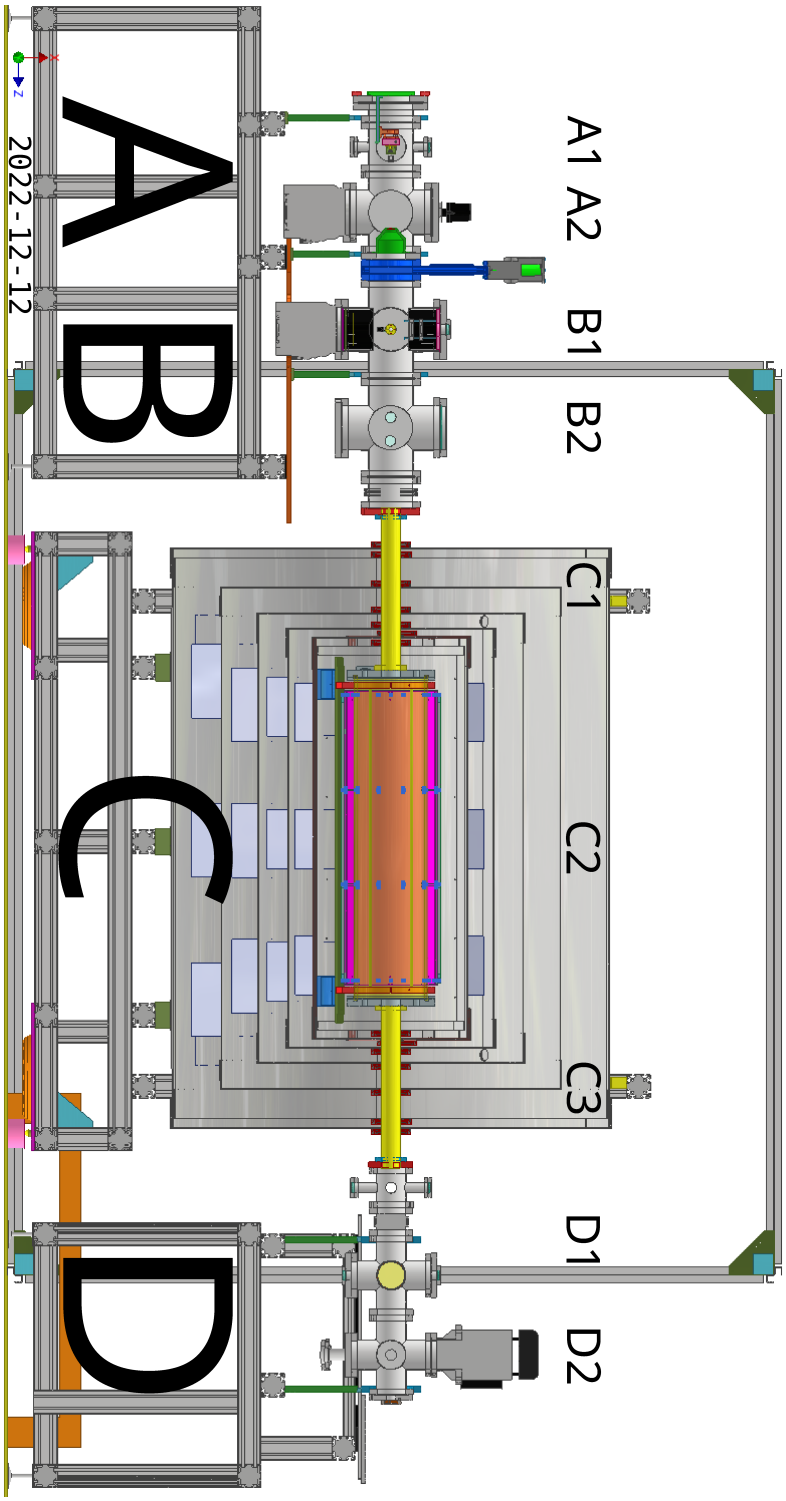

Figure 1: A schematic of the NL-eEDM set up. From the left, section **A** contains the source that emits the BaF beam, which is then collimated and cooled. In section **B**, the molecules are counted using LIF, before heading into the interaction zone **C**. In section C1, the molecules are optically pumped, and then they are probed for an electric field shift. In section **D**, the molecules are counted again using LIF at D1, and in D2, the counter propagating beam is aligned [14].

1.2 Motivation and Research Goal

This thesis is connected with the NL-eEDM collaboration, with the intent to investigate a potential method to improve the signal readout at section D1 in Figure 1. The analysed signal readout can be seen in Figure 2.

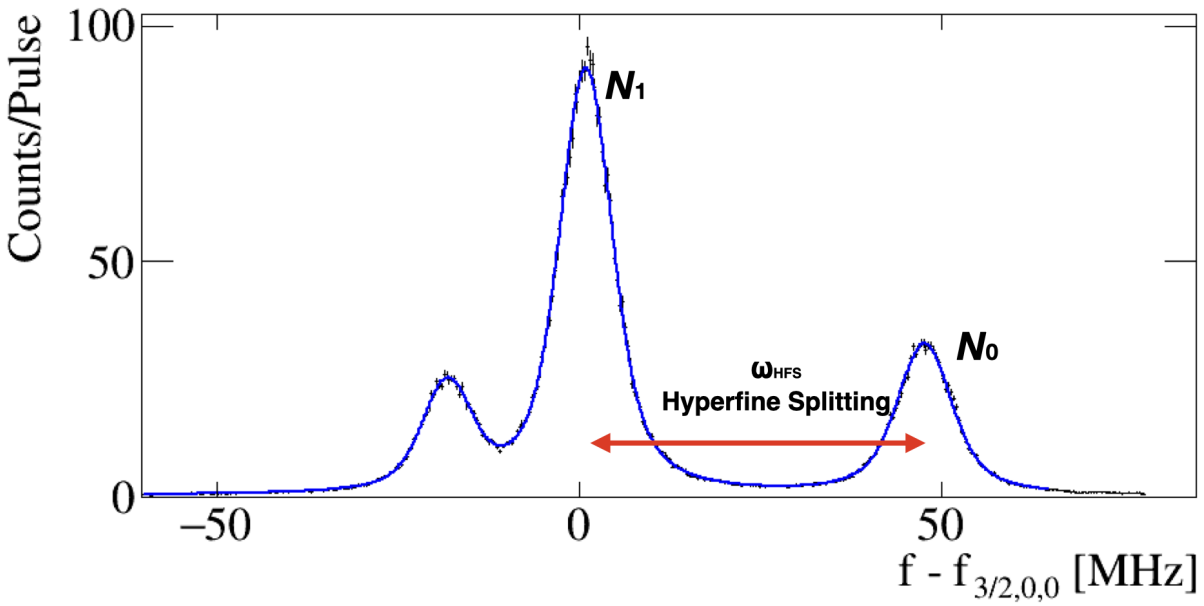

Figure 2: The normalised photon count rate of the $X^2\Sigma$ to $A^2\Pi_{3/2}$ transition as a function of probe laser frequency. The peaks labeled N_1 and N_0 correspond to the photons from the $F = 1$ and $F = 0$ molecular levels of the ground state.

The transition shown in the figure is the transition from the $X^2\Sigma$ to $A^2\Pi_{3/2}$ state, which has the following energy level structure:

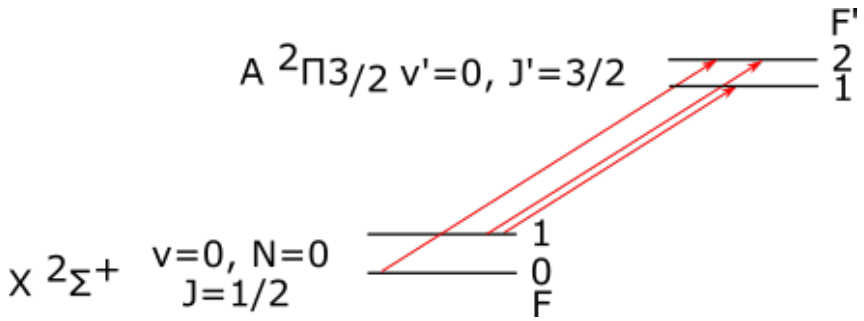

Figure 3: Energy level diagram of the $X^2\Sigma$ to $A^2\Pi_{3/2}$ transition. Figure from [15].

Figure 2 shows the distribution over F states coming out of the source, meaning that the figure would look different if another state was probed instead of the $N = 1$ state. There are three peaks, each corresponding to different hyperfine levels. The ones of interest are the peaks labeled N_1 and N_0, which relate to the $F = 1$ and $F = 0$ molecular levels of the ground state respectively. Due to the hyperfine splitting of the ground state and the excited state, there is a $\omega_{HFS} = 46.86$MHz frequency difference between these levels. This means that a laser beam

must be used to probe over the entire frequency range, which is not optimal.

From the importance of improving the signal readout in order to make a good precision measurement, the research question arises: **"Is it possible to use one laser to probe different frequencies simultaneously?"**

In this thesis it is shown that acousto-optic modulators (AOMs) can be used to 'create' a second beam, allowing for simultaneous probing of two different frequencies. Two methods, using different AOMs, are explored.

2 Theory

This section explains background physics concepts that are relevant to this thesis. First, the energy level structure of the BaF molecule is explained, as it is important for the LIF in the experiment. Then, the Lorentzian intensity distribution is explained, as the laser intensity in this experiment is often Lorentzian. Lastly, Gaussian beam optics are explained, since the experiment in this thesis uses laser light in fibers and in free space.

2.1 Energy Level Structure of BaF

The NL-eEDM experiment makes use of the molecular energy level structure of BaF in order to make an electron electric dipole experiment, and so it is important to understand some of the details to understand how the laser induced fluorescence takes place.

The experiment uses the the $N = 0$ level of the $X^2\Sigma_{1/2}$ ground state. The $F = 0$ and $F = 1$ hyperfine levels are split by a 65.86MHz frequency difference. The goal is to count the number of molecules that are in these hyperfine levels, which is done via laser induced fluorescence. Using laser light, the molecules in the ground state are excited to the $F = 1$ and $F = 2$ hypefine levels of the $A^2\Pi_{3/2}$ excited state. The lifetime of a molecule in this state is 47.9(7)ns for $A^2\Pi_{3/2}$ [17], meaning that a photon is emitted near instantly.

Due to the short lifetime, the molecule in the excited state will emit a photon in order to return to a more stable state. This could be either the ground state, or some other lower energy state.

The life time can be used to find the frequency line width, given by:

$$\Gamma = \frac{\gamma}{2\pi}, \tag{2}$$

here γ is the decay rate, the inverse of the lifetime. With the decay rate of $A^2\Pi_{3/2}$, the line width Γ is 3.32MHz, which is a very good resolution for the hyperfine splitting of the transition.

In the experiment, it is preferable that after the molecule emits the photon, it decays to a different energy level that is not the ground state. The exact state is not of particular importance, since there are several possible molecular states. Returning to the $N = 0$ ground state however can add some additional complications that have to be accounted for. Very few of the excited state molecules return to the $N = 0$ ground state (the dotted purple line in Figure 4)

due to molecular selection rules, and most move to the $N = 2$ state [18], as shown by the solid purple arrow in Figure 4. Full analyses of the energy level structure of BaF and the molecular decays can be found in [18], [19].

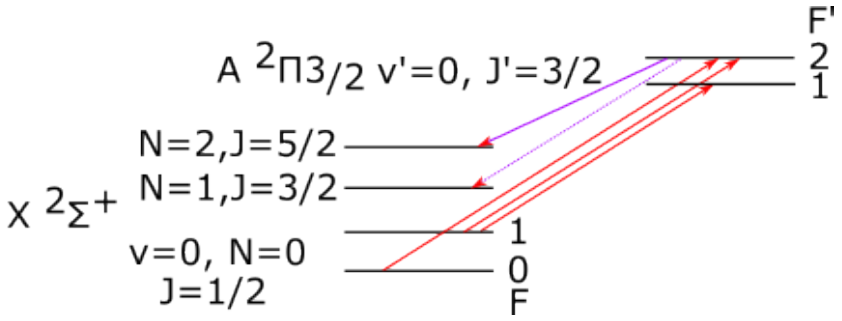

Figure 4: Energy level diagram of the $X^2\Sigma$ to $A^2\Pi_{3/2}$ transition, also showing the $N = 1$ and $N = 2$ levels of the $X^2\Sigma$ state. The purple arrows depict a decay. Figure adapted from [15]. Figure not to scale.

2.2 Lorentzian Intensity Distribution

While the intensity distribution of a laser beam out of a fiber is often Gaussian, the intensity as a function of laser frequency can be detuned from the centre frequency, which can be accounted for using a Lorentzian distribution of the form:

$$\mathcal{L}(\omega) = \frac{s_0}{2 * (1 + s_0 + \frac{\delta^2}{\gamma})}. \tag{3}$$

Here ω is the laser frequency, s_0 is a saturation coefficient, δ is the laser frequency detuning, and γ is the decay rate of the molecule:

$$\gamma = \frac{1}{\tau}. \tag{4}$$

Here τ is the lifetime of the molecule in the excited state, as explained in section 2.1.

The laser frequency detuning δ is defined as:

$$\delta = \omega_L - \omega_0. \tag{5}$$

Here ω_L is the detuned frequency, and ω_0 is the centre laser frequency (analogous to the μ term in the Gaussian distribution).

2.3 Gaussian Beam Optics

Laser beams (such as those coupled to single-mode fibers) are in the form of Gaussian beams, which means their intensity can be written as a Gaussian function [20]:

$$f(z) = A \exp\left(-\frac{(z-\mu)^2}{2\sigma^2}\right). \tag{6}$$

Here A defines the height of the Gaussian curve's peak, μ is the position of the centre of the peak, and σ is the standard deviation of the Gaussian, which describes the width of the curve.

The intensity function is then just a variation of this standard Gaussian, and can be written in physics terms [21]:

$$I(r,z) = \frac{2P}{\pi w(z)^2} \exp\left(\frac{-2r^2}{w(z)^2}\right). \tag{7}$$

Here P is the total power of the laser beam, $w(z)$ is the radius of the laser beam where the irradiance is a fraction of the peak irradiance I_0, r is the radial distance from the axis, and z is the distance propagated from the plane where the wavefront is flat.

As the beam propagates through space, the irradiance profile does not stay constant, it converges and diverges by an angle θ from the beam waist w_0 (position where the beam diameter reaches $1/e^2$ of the maximum value). The divergence angle and the beam waist are related by the expression:

$$w_0 = \frac{\lambda}{\pi\theta}. \tag{8}$$

Here λ is the wavelength of the laser.

The beam radius $w(z)$ is then described by the following equation:

$$w(z) = w_0\sqrt{1 + \left(\frac{z}{z_R}\right)^2}. \tag{9}$$

Here z_R is the Rayleigh length, defined as the distance along the propagation direction of the beam from the waist to the position where the cross-section area doubles. It is described by the expression:

$$z_R = \frac{\pi w_0^2}{\lambda}. \tag{10}$$

The Rayleigh length determines the length that the beam can propagate without significant divergence [22], so a large Rayleigh length implies a more collimated beam. It is important in this experiment for the laser beam to stay collimated over a sufficiently large distance (on the order of 10cm), such that it stays collimated and focused inside the AOM and the output beams remain collimated. This also makes it easier to couple the output beams into a fiber again.

Using Equation 10 and the parameters from the experimental set-up (see section 4), the Rayleigh length is calculated. The beam diameter of the beam can be found in [23]. The result of this calculation can be found in table 1. It is clear that the laser beam will stay collimated through the AOM.

Table 1: Rayleigh length calculation using parameters from the experimental setup

Laser Wavelength (λ)	Beam Width (w_0)	Rayleigh length (z_R)
815nm	1.62mm	10.12m
		$z_R = \frac{\pi w_0^2}{\lambda}$

3 Laser Induced Fluorescence (LIF) and Depletion of Molecules

In the NL-eEDM experiment, the molecules are counted using laser induced fluorescence, where the molecule is excited from the ground state to the $A^2\Pi_{3/2}$ state using a laser, which then leads to the emission of a photon that can be counted using a PMT.

The LIF considered in this section is the one that happens at section D1 of the experiment in Figure 1, 3840mm from the BaF source.

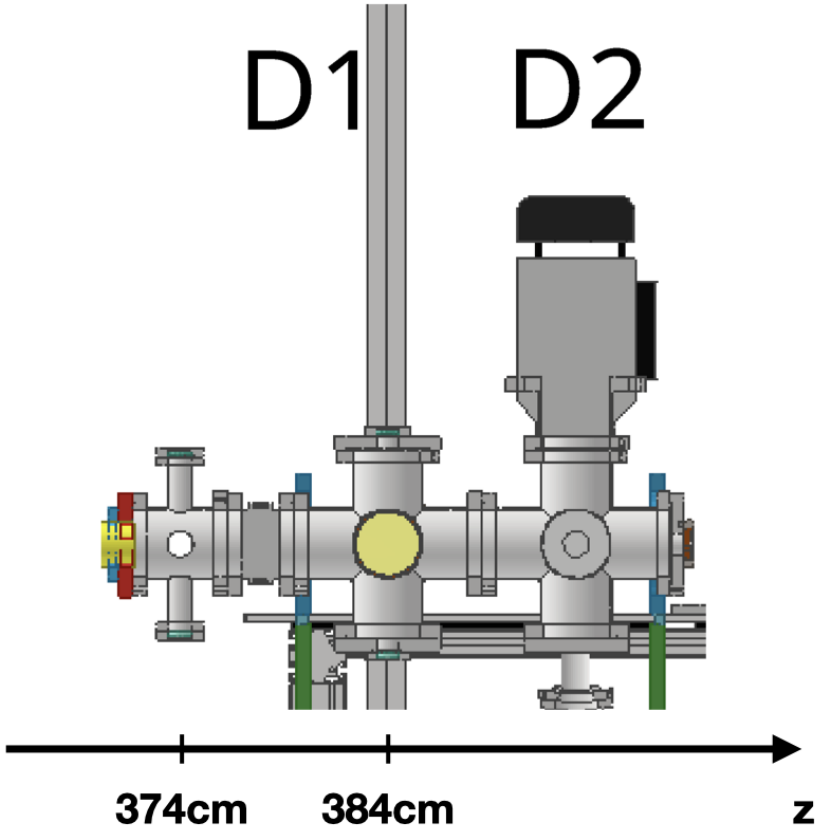

Figure 5: A zoom in to section D of the experiment, where the LIF takes place in the region with the yellow circle. Image adapted from [14].

Here, the BaF beam travelling with a velocity of 600m/s passes through a laser field of width 2mm [24] orthogonal to the BaF beam [16] as shown in Figure 6. It is ideal for this laser field to be Gaussian, however it may not be. The exact distribution of the laser intensity may not be known, it can be measured.
Once the intensity distribution is understood, the depletion of the molecules can be modelled using the method described below, in equation 11. If the laser field is at an angle with respect to the beam, then there is a Doppler shift that needs to be accounted for. Therefore, this angle should be small.

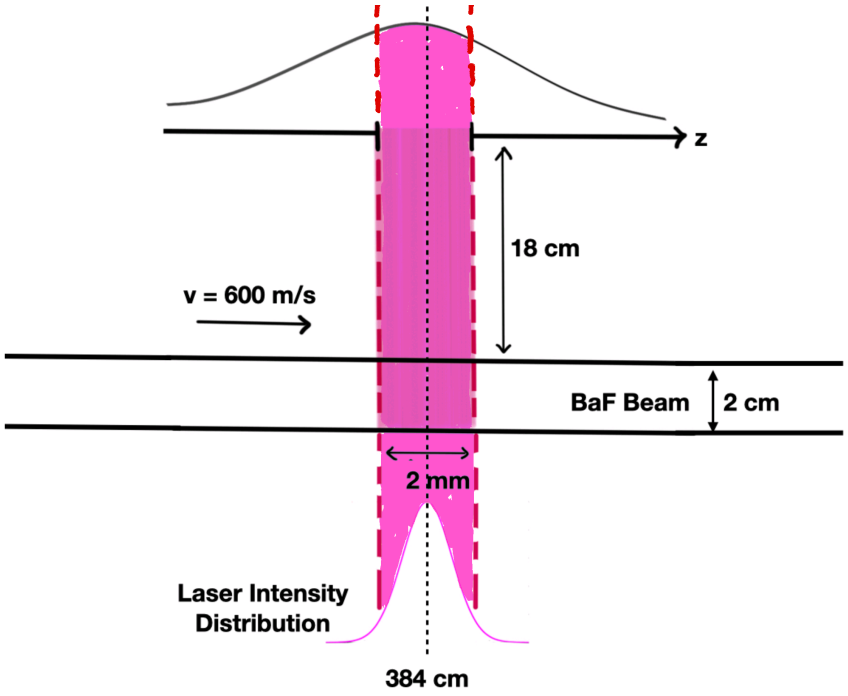

Figure 6: A schematic of the BaF beam passing through the laser field. The laser field (in pink) is perpendicular to the beam, at a distance of 3650mm from the supersonic source (indicated via the z-axis). The laser light passes through the aperture at the top of the schematic, and has a Gaussian distribution, for depiction purposes. The distances depicted are not to scale.

3.1 Modelling the Depletion

The number of molecules and thus the number of photons gets depleted as the molecules pass through this laser field, given by the function:

$$N(z) = N_0 - \int_{-\infty}^{z} \alpha I(z) N(z) dz. \tag{11}$$

Here N_0 is the initial count of molecules, α is the probability of exciting the molecule to the intended molecular level such that it releases a photon, and $I(z)$ is the intensity distribution (this is often a Gaussian or Lorentzian, but could also be different) of the laser. Since LIF is also done at Section B of the experiment (refer to Figure 1), the initial number of molecules can be counted, allowing for the calculation of the depletion.

Equation 11 can also be written in the form of a differential equation of the form:

$$N^{'} = \alpha I N. \tag{12}$$

Here N' is the first derivative of the number of molecules.

Based on the above equations, a method is developed to model the depletion of the molecules as they pass through the laser field, which accounts for different types of intensity distributions and and intensities, and laser detuning, as can be seen in Figure 7. The model allows for easy

variation of several different parameters, including the width and position of the intensity distribution. This model can then be expanded to account for two laser fields, such that both the $F = 1$ and $F = 0$ states can be probed. The detuning component of the model would also then be able to show the influence of the second laser field on the other state and vice versa.

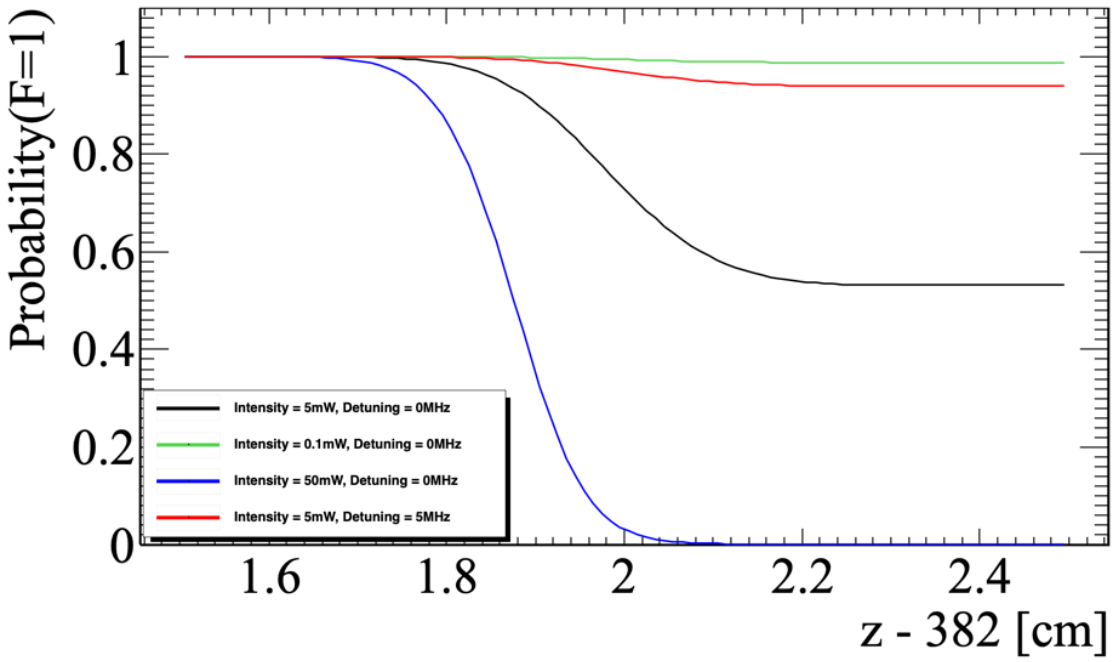

Figure 7: Simulation of the depletion function of the $F = 1$ state, with different intensities and detuning. The laser beam is centred at 2cm for demonstration, and its width is set as 2mm.

From Figure 7 it can be seen that when the laser is detuned (the red curve) from the centre frequency, or the intensity is too small (the green curve), not all the molecules are depleted as the beam passes through the laser field. If the laser intensity is too large (the blue curve), the molecules get depleted instantly instead of at the peak of the intensity distribution.

The number of photons emitted by the molecular depletion is then given by:

$$N_\gamma = P_{ext} * N_M. \tag{13}$$

Here N_γ is the number of emitted photons, P_{ext} is the probability that the molecule has been depleted, and N_M is the number of molecules.

However, not all of these photons are detected by the PMT, since those have their own efficiencies. The number of photons corresponding to any one molecular level (for instance the $F = 1$ level) is then given by:

$$N_{F=1} = \varepsilon N_\gamma. \tag{14}$$

Here ε is a combined efficiency term of the PMT that is given by:

$$\varepsilon = \Omega * \mathrm{QE} * \mathrm{transmission}. \tag{15}$$

Here Ω is the solid angle (on the order of 10^{-2}), QE is the quantum efficiency of the PMT (around 0.15), and transmission is the transmission coefficient of the PMT (about 0.8). The equations are the same for the $F = 0$ molecular level, since it is just one laser probing over the entire frequency range. Research can be done in order to optimise the number of photons detected, such as alternatives to PMTs in order to improve the quantum efficiency, as in [25].

Using equations 13 and 14, the number of molecules in a certain F state can be calculated, which is useful in order to make an eEDM measurement.

The laser power cannot be increased too much in order to increase the total number of photons that could be counted by the PMT, as this can saturate the depletion, such as the blue curve in Figure 7. While this would increase the total number of photons, there will be far more background light (N_{BG}) photons than photons from any of the molecular levels (N_F), which worsens the signal to noise ratio given by:

$$SNR = \frac{N_F}{\sqrt{N_{BG} + N_F}}. \tag{16}$$

It is important to note that the number of background photons N_{BG} is directly proportional to the integral of the intensity distribution, and not just the total intensity:

$$N_{BG} \propto \int I(z)dz. \tag{17}$$

To stay within the regime where $N_F > N_{BG}$ (good signal to noise ratio), and to not deplete all the molecules at once, it is found that the laser intensity should be on the order of 1mW/cm^2.

Further details on the signal to noise ratio and the counting statistics of molecules in the NL-eEDM experiment can be found in [26].

3.2 Conclusion

At section D1, the molecular beam passes through a laser field, causing the molecules to get depleted and emit a photon. A method has been developed to model different laser intensity distributions and this depletion, in a manner that can account for laser detuning. This method can be expanded to include a second laser field at a different frequency, allowing for simultaneous modelling of the $F = 0$ state evolution. The detuning factor can investigate any cross-talk between these two laser fields, and see the effect of both fields on both molecular states.

The code for this method can be found in Appendix A.

4 Experimental Design and Procedure

Before moving on to the experimental design, the requirements to answer the research question must be established.

The primary objective is to have a ω_{HFS} frequency difference between the two laser fields. To be implemented in the experiment without worsening the signal to noise ratio and depleting all the molecules at once, the intensity of both these laser fields should be on the order of $1\text{mW}/\text{cm}^2$ (see section 3). To use the same laser to create two laser fields at different frequencies, the frequency modulation would have to take place in free space as opposed to in optical fibers. The two laser beams must then be coupled back to fibers to be used in the experiment. This means that there must be sufficient spatial separation between the two laser beams in free space, such that they can be separated and fiber coupled.

4.1 Acousto-Optic Modulators (AOMs)

An acousto-optic modulator is a device that can be used to control the transmitted power of a laser beam, and also modulate the frequency and spatial direction of the beam. They use the acousto-optic effect, where the refractive index of a material (usually glass) is modified using the mechanical strain of a sound wave [27]. In order to make sure a diffracted beam is created and goes out of the AOM, the AOM must be aligned such that it is at an angle to the input beam, as can be seen in Figure 8.

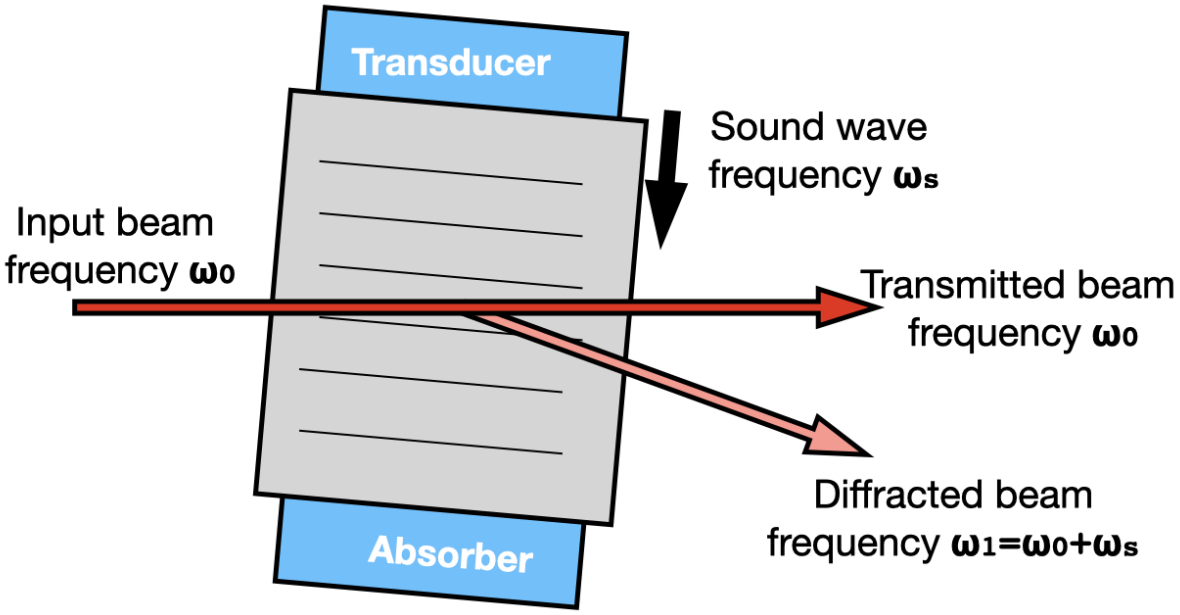

Figure 8: A schematic of a non resonant AOM, showing the working principle as well as the frequency modulation mechanism. The angular separation between the transmitted beam and the diffracted beam is exaggerated for demonstration purposes.

Using a radio frequency (RF) input to a transducer, a sound wave is generated inside the AOM, and the laser beam is diffracted off this wave, shown in Figure 8. The frequency of the diffracted

laser beam is the sum of the input beam frequency and the sound wave frequency, and the diffracted beam propagates in a slightly different direction (with a small angular separation).

The transmitted beam is often called the “0th order beam", and the first diffracted beam is referred to as the “1st order beam". Some AOMs can produce several higher order beams, if they are in the Raman-Nath regime, but most AOMs function in the Bragg regime where there is a large diffraction efficiency for the first order beam and very little for any further order. The diffraction efficiency is defined as the ratio between the 1st order beam power and the input beam power. Most AOMs have a high diffraction efficiency.

Since AOMs can be used for power and frequency modulation, and create a spatial separation between the transmitted 0th order beam and the diffracted 1st order beam, they could be a good choice to allow for creating two laser fields of different frequencies, allowing for simultaneous measurements.

4.2 AOM Set-up Design

In order to investigate whether AOMs are a viable choice to answer the research question, two similar versions of a set up were built, featuring two different AOMs in order to compare them. This section aims to justify the choice of set-up, and also describe it.

Table 2: A list of the devices and apparatus used to construct the experimental set-ups, along with relevant information about these items.

Item	**Quantity**	**Specification**	**Relevant Information**
RF Power Supply	1	Hewlett Packard 8657A Signal Generator 0.1-1040 MHz	RF source 1
	1	Rigol DG4202 Function/Arbitrary Waveform Generator 200MHz	RF source 2
RF Amplifier	1	EN Model 601L RF Power Amplifier	1.2 Watts Linear 37 dB amplification
Photodiode	1	Thorlabs SMO5PD2B	
AOMs	1	Brimrose 10 TEM-240-50	Centre Frequency: 200MHz Bandwidth: $(170-230)$MHz
	1	IntraAction AOM-402AF1	Centre Frequency: 40MHz Bandwidth: $\pm(30-50)$MHz
Mirrors	2	Thorlabs EO3	Broadband dielectric mirror
	2	Thorlabs PO1	Silver coated mirror
	1	Thorlabs BBD1-E03	D-shaped mirror
Lens	1	Thorlabs LB1437-B	Focal length : 150mm
Fiber Coupler	2	Thorlabs PAF2-7B	Effective Focal Length: 7.5mm
Laser Viewer Card	1	Thorlabs VRC5	

In general, for both the set-ups, it was important to align the AOM properly, as any changes in alignment could change the output beams. Poor alignment could result in no output whatsoever.

Bad alignment could lead to no 1st order beam being created, or the beam being only partially diffracted, meaning that the 1st order and 0th order beams would no longer be Gaussian or have the maximum possible intensities, which would create problems when coupling back to fiber.

4.2.1 Using a 200MHz AOM

First, a set-up was built featuring a 200MHz centre frequency AOM. Due to the large frequency range, it was possible to use two radio frequency sources simultaneously to create two first order beams, each with a controllable frequency independent of each other. To do this, two RF sources were input into an RF amplifier, and the output was sent to the AOM. RF source 1 was set to 225MHz, with a RF power of 16dBm. RF source 2 was set to 177MHz, with a RF power of 10dBm. dBm can be converted to units of mW using this table.

With these RF power inputs, the entire bandwidth of the AOM is in use (see Table 2), meaning that there is less room for error and alignment.

The two first order beams then have a 48MHz frequency difference which can be used, while the 0th order beam can be reused for some other purpose. To ensure that the output powers are similar, the RF powers on the two sources should be comparable or equal to each other. In order to achieve this, a 16dB attenuator was attached to RF source 2 (Figure 9), the Rigol DG4202.

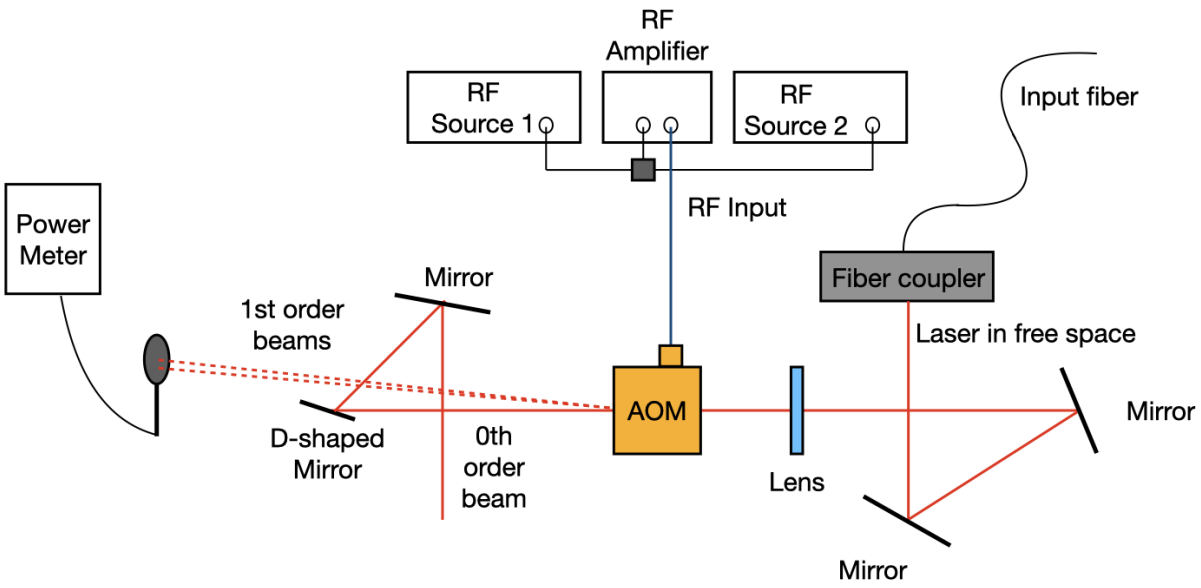

Figure 9: A schematic of the set-up using the 200MHz AOM, to be observed from right to left. Two radio frequencies are input into an amplifier, and the output of the amplifier in sent into the AOM. Two first order beams are created, allowing for the 0th order beam to be picked off using a D-shaped mirror. The power meter is used to measure the output powers of the first order beams.

Once the laser light has been coupled out of the fiber into free space using a fiber coupler, it is aligned to be perpendicular and collimated out of the fiber, with a power output $P_O = 3.42$mW. The laser beam is then reflected off two mirrors, which adds two degrees of freedom and thus

allows for better fine-tuning of the beam. Before the beam goes into the lens, it is passed through a focusing lens. This is to ensure the beam actually goes through the AOM aperture. The focal length of the lens is chosen such that the focus is at the centre of the AOM crystal. Here, a 150mm focal length lens was chosen as it yielded better results than other lenses without having to realign the entire set up.

Table 3: Table summarising the power inputs used for the 200MHz AOM set up. It is important to note that these are the power outputs of the sources themselves, prior to power amplifications from the attenuator and the amplifier.

RF Source 1	Frequency	225 MHz
	Output Power	16 dBm
RF Source 2	Frequency	177 MHz
	Output Power	10 dBm

Three beams go out of the AOM, the 0th order beam, and two first order beams. Since the 0th order beam is of no interest to this research in this case, it can just be separated from the set-up using a mirror, and can be coupled back into a fiber for any other purpose. Due to the focusing lens however, the beam diverges as it propagates out of the AOM, so another lens will be needed to collimate the beam again.

The laser power of the two first order beams is measured using a power meter, both at the same time, with enough spatial separation between the beams, and with just one RF input at a time. This allows for the study of the power dependency and the impact of one RF power on the other 1st order beam. The 1st order beams can then be coupled back into fiber the same way as light is coupled out of a fiber, using two mirrors for control and then focused into a fiber coupler, but this was not done with this set up.

4.2.2 Using a 40MHz AOM

A similar set-up and study was done using an AOM with a 40MHz centre frequency. A major difference here is that only one RF source is used with the frequency set to 48MHz, in order to create a ω_{HFS} frequency difference between the 0th order beam and the 1st order beam.

The set up was kept largely the same and only the AOMs were swapped. The focusing lens was found to be unnecessary, due to the larger aperture of this AOM, and the fact that the laser beam was well collimated. The Rayleigh length was calculated to be large enough that the beam would easily stay collimated over the entire set-up length (see section 2.3).

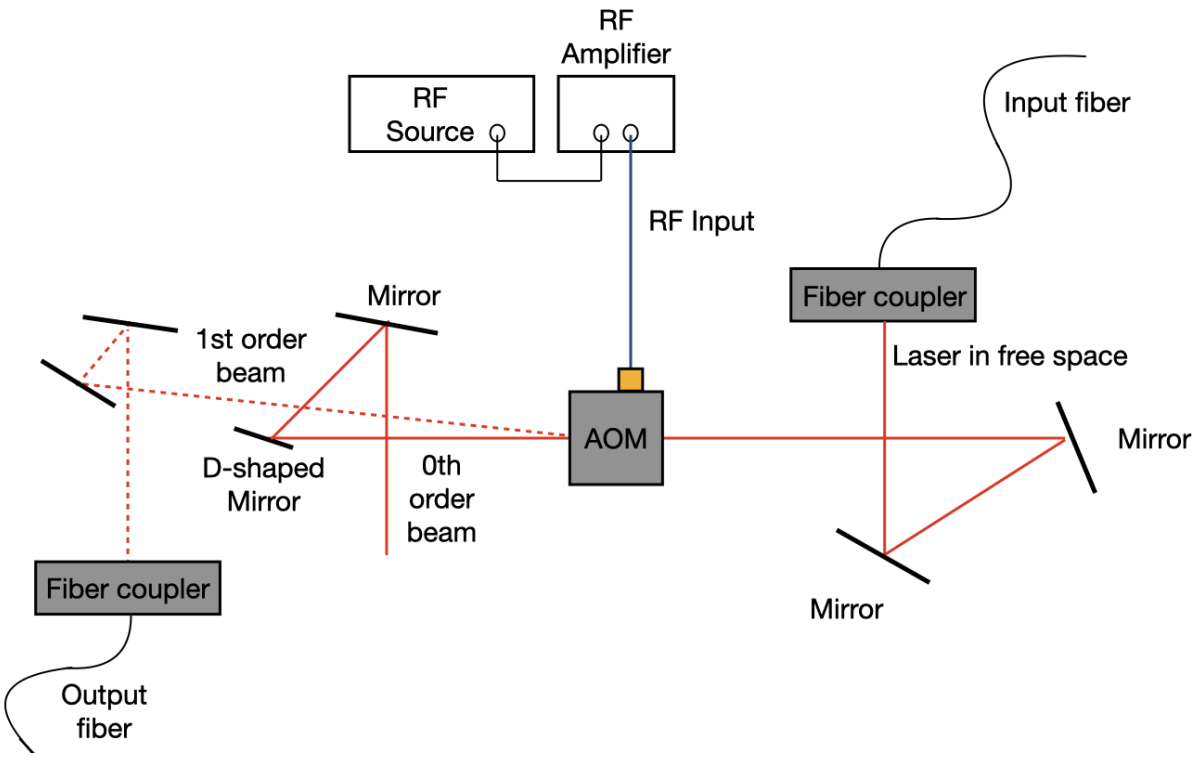

Figure 10: A schematic of the set-up using the 40MHz AOM, to be observed from right to left. Only one radio frequency is input into the AOM, so the 0th order beam is picked off with the intention to also couple into a fiber, and the first order beam is coupled into a fiber.

Since there is only one input radio frequency into the AOM, there are only two output beams, the 0th order beam and the 1st order beam. The high diffraction efficiency of the AOM ensures that higher order beams are either not created at all or have a negligible power compared to the 0th and 1st order beams. The separation of the beams was observed using a detector card, and then they can be measured and separated to allow for fiber coupling.

4.3 Conclusion

The goal with the 200MHz AOM was to investigate whether the two 1st order beams will have enough spatial separation in order to separate them and couple to fiber, and to investigate the power output. The spatial separation is checked for by eye, using the Thorlabs VRC5 IR detector card. However, it could also be done using an IR camera and then analysed using a similar method as described in [28].

The goal with the 40MHz AOM set up was similar: investigate the power outputs and the spatial separation of the two beams, to see whether they would be good to use for LIF. The powers of the beams were first measured using a power meter.

The two set-ups and their results are then compared, to see which one is better to use (see Section 5). It is important that a quantitative measurement is carried out, such that the set-up can be implemented (see Section 3).

5 Results and Discussion

This section shows and compares the results from the two AOM set-ups. These results are the visual spatial separation of the beams from each other, as can be seen in a picture of the detector card, and the power outputs of the beams. After comparison, an AOM is recommended for use in the main experiment.

5.1 200MHz AOM

First, the output powers of the 1st order beams were measured independently of each other. The power of the 0th order beam was not measured, since it was not intended to be used.

Using RF source 1 with the frequency and input power described in table 3, and an input laser power P_O, the power of the 1st order beam was measured to be 0.454 ± 0.001 mW.

Using RF source 2 with the frequency and input power described in table 3, and an input laser power P_O, the power of the 1st order beam was measured to be 0.094 ± 0.001 mW.

Pictures of the IR reader card were taken to show the separation of the 1st order beams from the 0th order beam, first individually and then with both sources switched on.

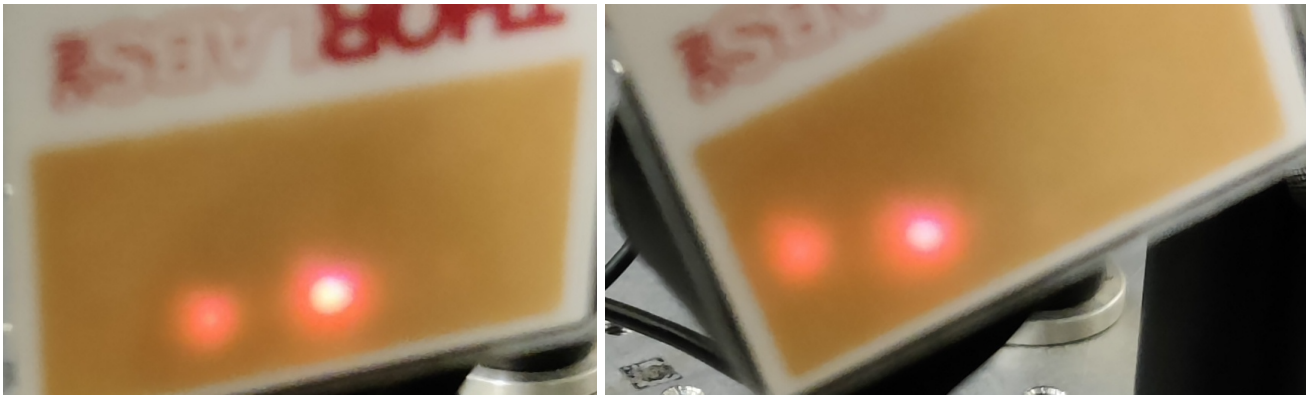

(a) 0th and 1st order beams from RF source 1. (b) 0th and 1st order beams from RF source 2.

Figure 11: Pictures of the 0th and 1st order beams from the two RF sources individually, with the 1st order beam on the left and the 0th order beam on the right. It can be seen from the brightness that the 0th order beam has much higher power than the 1st order beam.

It can be seen from Figure 11 that the separation of the 1st order beams from the 0th order beam is clear, and around 1cm, which is enough to work with.

Then, both RF sources were switched on with the specifications described in Table 3, and a picture was taken, without changing the original alignment of the AOM.

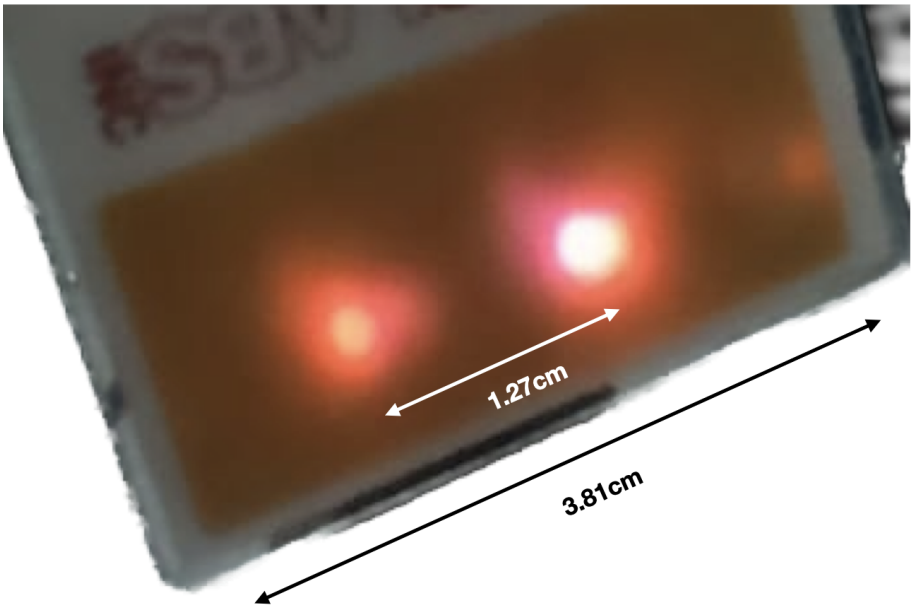

Figure 12: A picture of the IR reader card with both RF sources turned on using a 200MHz AOM. The 1st order beams are on the left, and the 0th order beam is on the right.

In Figure 12, the two 1st order beams are created. There is some visible light to the far right of the reader card, showing that there was either an issue with alignment, or one of the 1st order beams did not diffract correctly when both the sources were input into the AOM. By eye, it can be seen that there is little to no visible separation between these two beams. It is possible to quantify this separation using the method described in [28], however, it makes sense to look for separation by eye in order to align the D-shaped mirror and attempt to reflect one of the 1st order beams.

Based on this, it was decided to not attempt to separate the two 1st order beams and couple them to fibers, since by eye it appears difficult to do. Additionally, the low power of these beams present another challenge, since powers on the order on 1mW are needed for a suitable LIF measurement of the molecules, and there is also some power lost when the laser beam is coupled into a fiber, reducing the power even further.

5.2 40 MHz AOM

Similar to the 200MHz AOM set-up, the power outputs of the beams were first measured. With a radio frequency of 48MHz and a power of 16dBm, the power of the 0th order beam was measured to be 1.30mW and the power of the 1st order beam was found to be 2.11mW.

Table 4: Summary of power outputs with constant RF frequency 48MHz and RF power.

Input (dBm)	0th Order Power (mW)	1st Order Power (mW)
16	1.30	2.11

Then, a picture of the IR reader card was taken in order to demonstrate the separation of the two beams from each other.

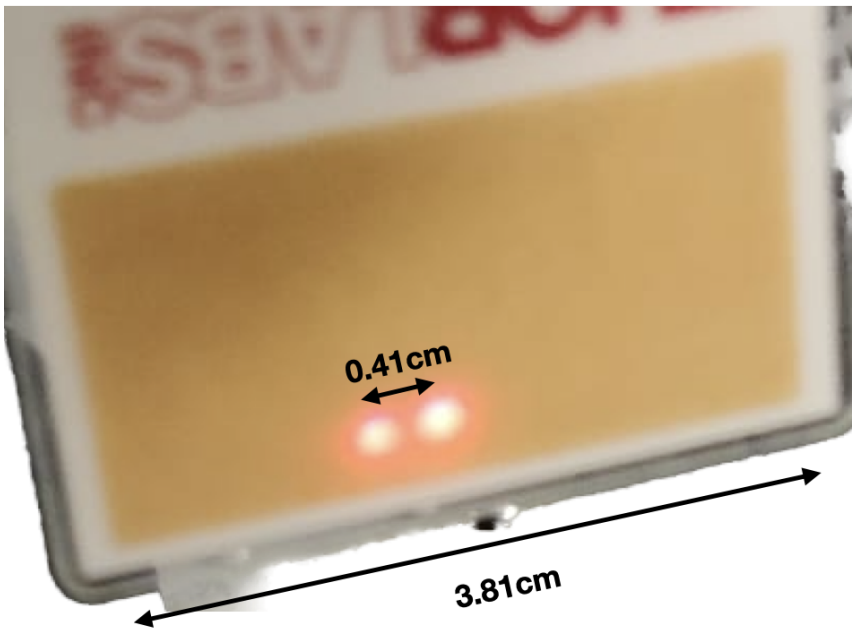

Figure 13: A picture of the IR reader card showing the separation of the 1st order beam from the 0th order beam. On the left is the 0th order beam, and on the right is the 1st order beam.

From Figure 13, a clear spatial separation can be seen between the two circular output beams, allowing for one of them to be reflected away using a D-shaped mirror. Once the 0th order beam was reflected away, the 1st order beam can be coupled to a fiber.

5.3 Comparison of AOM Set-ups

The 200MHz AOM yielded low powers and had poor separation between the two first order beams. However, the two first order beams are largely independent of each other in terms of their powers, so changes in one RF power does not have much impact on the other beam. However, this was difficult to measure and accurately quantify due to the lack of separation of the two first order beams. There is also a limitation on the RF power that can be supplied at the moment, meaning that the only possible methods of optimising the power output is by optimising the alignment of the set-up.

The 40MHz AOM yielded a 0th order and 1st order beam with fairly comparable powers that are in the right range of powers. Any change in the radio frequency power will have significant changes on the powers of both beams, but primarily on the 1st order beam. While this could be a cause for concern, it is easily controllable, since the input fiber only outputs half of the power of the laser, by means of a fiber splitter. This means that only the 1st order beam needs to be fiber coupled, and the 0th order beam can be used either for LIF, or for some other purpose.

Hence, the 40MHz AOM is recommended for further use and implementation, since it satisfies all the requirements listed in Section 4 with the best results.

6 Conclusion

The aim of this thesis was to investigate a potential method to improve the signal readout of the NL-eEDM experiment, which aims to make a sensitive measurement of the electric dipole moment of the electron using a beam of BaF to a sensitivity of $d_e < 5 \cdot 10^{-30}$ e cm. In the signal readout, there are two major peaks of count rate as a function of frequency, each corresponding to a hyperfine level of the $N = 0$ ground state of the BaF molecule. There is a frequency difference of ω_{HFS} between these two peaks.

The molecules in the experiment are counted using laser-induced fluorescence (LIF), where the molecules are excited to a higher molecular state ($A^2\Pi_{3/2}$) using a laser beam, which causes the molecule to emit a countable photon. A method has been developed to model the molecular depletion with different laser intensities and distributions, and detuning. This model should be expanded to allow for a second light field.

Acousto-optical modulators (AOM) were identified as a potential method to create a second laser beam, allowing for both frequency peaks to be probed simultaneously. AOMs use the acousto-optic effect (a radio frequency input to create a sound wave that light can diffract off) to diffract an input beam and create a second beam. In order to investigate whether AOMs are suitable for use in the NL-eEDM experiment, two set-ups are built, using two different AOMs, one with a centre frequency of 200MHz, and one with a centre frequency of 40MHz.

Two independent radio frequencies were input into the 200MHz AOM, in order to create two first order beams. These first order beams were found to have low powers and more importantly, little to no separation between them, making it difficult to separate them and couple them into fibers, or to make more quantitative statements on the influence of one radio frequency on the other in terms of output power.

A 48MHz radio frequency was directly input into the 40MHz AOM. It was found that there was good separation between these two beams, and the powers of the beams were comparable and in the right range for use in the main experiment.

It can first be concluded that an AOM can indeed be used to create a second laser beam with a ω_{HFS} frequency difference and the required laser powers, which can be used in the main experiment to probe at different frequencies simultaneously.

It is recommended to optimise and use the 40MHz AOM and set-up, with some changes that could be made. This is because the power of the beams is on the order of 1mW, which is what is needed for LIF in the main experiment, and there is enough spatial separation between the beams to couple them into fibers.

6.1 Future Outlook

At the moment, the 40MHz AOM set-up remains built and can be used. The 0th and 1st order beams must first be coupled into fibers.

The intention is to then implement this into the NL-eEDM experiment by adding a new ap-

paratus to D1 in Figure 1. This apparatus, built in-house with commercial opto-mechanics, allows for two fiber inputs which are then coupled into free space and enlarged, and then passed through apertures. The light passing through the apertures are then reflected, and directed using a prism into the set-up. The prism can be tinkered with to allow for different spatial separations [24].

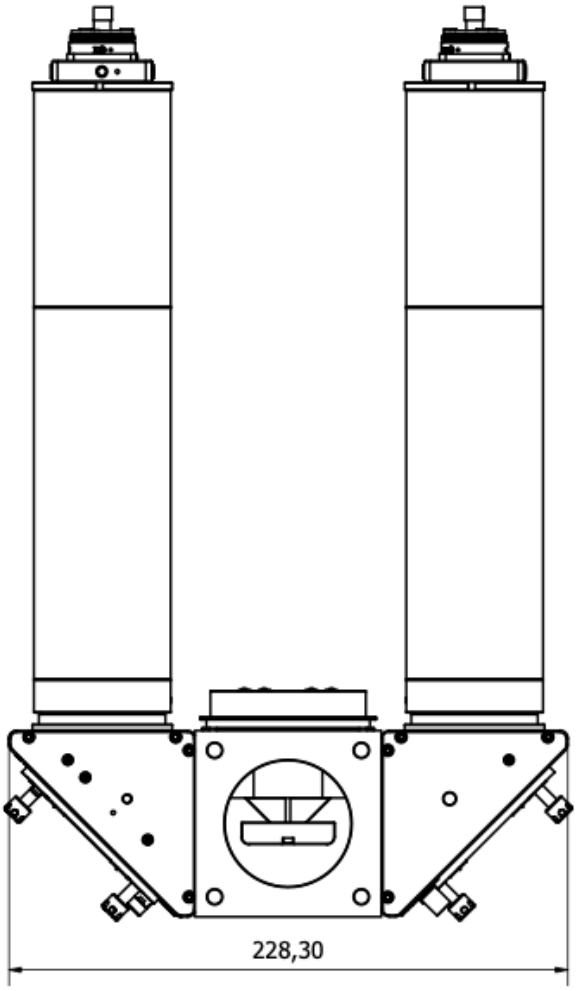

(a) A schematic of the apparatus [24].

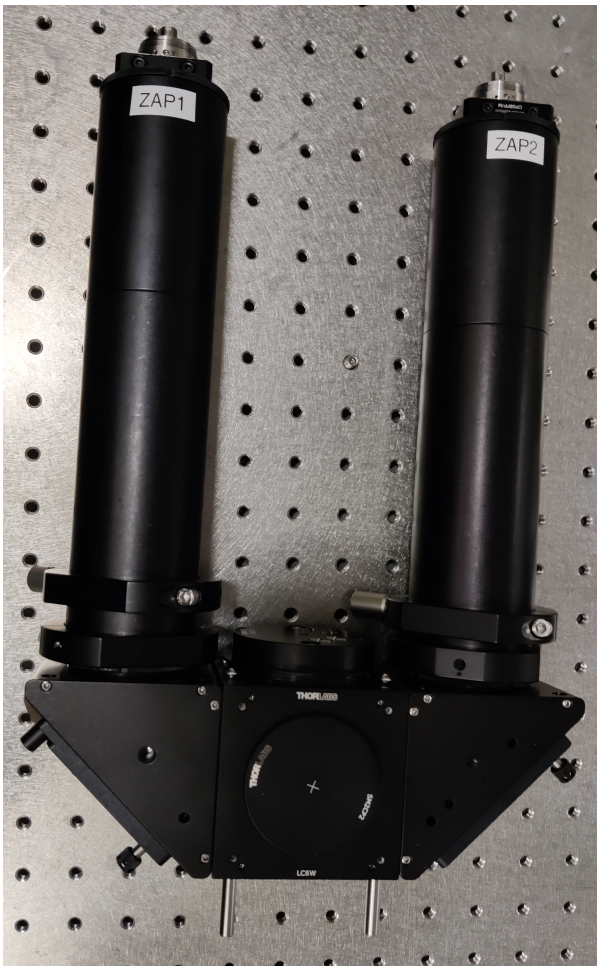

(b) A picture of the apparatus.

Figure 14: A schematic and a picture of the double slit assembly. At the top, there are two fiber couplers (ZAP1 and ZAP2). The laser beams are enlarged using lenses and directed through the tubes, and passed through an aperture. They are then directed to a prism, and then out.

Zooming into the figure to see the prism:

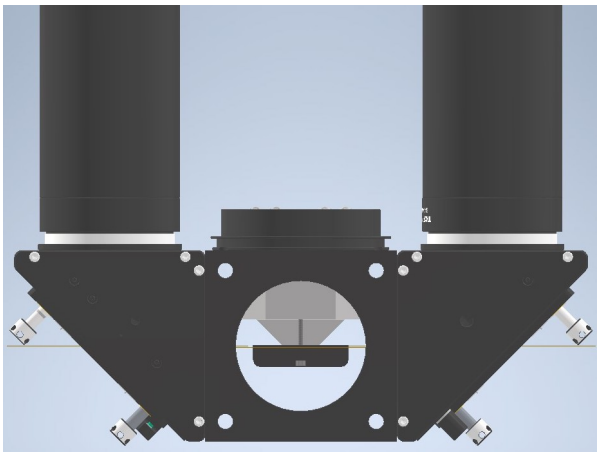

(a) A zoom in of the 3D model of the assembly, such that the prism can be seen [24].

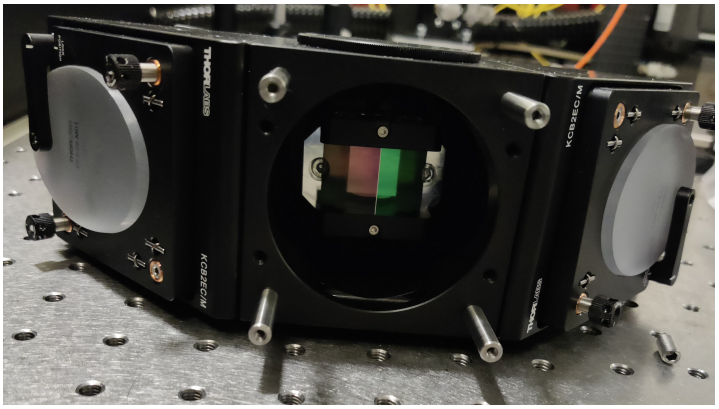

(b) A picture of the prism within the apparatus.

Figure 15: A 3D model and a picture of the double slit assembly zooming into the prism.

Once the apparatus has been implemented, it can be tested whether the system actually works within the NL-eEDM experiment as intended.

7 Acknowledgements

I thank Lorenz Willmann for supervising me through this project, providing a lot of feedback and all the discussions about not just my project but about the eEDM experiment as a whole, and for the useful life advice. I would like to thank the fast beam NL-eEDM group: Anno, Alexander, Ginny, Roman, and Thomas, for their support and their assistance whenever I needed it. I would also like to thank Oliver Böll for assistance in the lab and for providing useful schematics, and Aiva Misevičiūtė for some assistance with the sketches in this report.

References

[1] P. Aggarwal, H. L. Bethlem, A. Borschevsky, *et al.*, "Measuring the electric dipole moment of the electron in BaF," *The European Physical Journal D*, vol. 72, no. 11, Nov. 2018. DOI: 10.1140/epjd/e2018-90192-9.

[2] E. Purcell and N. Ramsey, "On the possibility of electric dipole moments for elementary particles and nuclei," *Physical Review*, vol. 78, no. 6, p. 807, 1950. DOI: 10.1103/PhysRev.78.807.

[3] T. D. Lee and C. N. Yang, "Question of parity conservation in weak interactions," *Physical Review*, vol. 104, pp. 254–258, Oct. 1956. DOI: 10.1103/physrev.104.254.

[4] C. S. Wu, E. Ambler, R. W. Hayward, D. D. Hoppes, and R. P. Hudson, "Experimental test of parity conservation in beta decay," *Phys. Rev.*, vol. 105, pp. 1413–1415, 4 Feb. 1957. DOI: 10.1103/PhysRev.105.1413.

[5] M. Pospelov and A. Ritz, "Electric dipole moments as probes of new physics," *Annals of Physics*, vol. 318, no. 1, pp. 119–169, 2005, Special Issue, ISSN: 0003-4916. DOI: 10.1016/j.aop.2005.04.002.

[6] Y. Ema, T. Gao, and M. Pospelov, "Standard model prediction for paramagnetic electric dipole moments," *Phys. Rev. Lett.*, vol. 129, p. 231 801, 23 Nov. 2022. DOI: 10.1103/PhysRevLett.129.231801.

[7] K. Jungmann, "Searching for electric dipole moments," *Annalen der Physik*, vol. 525, pp. 550–564, 2013. DOI: 10.1002/andp.201300071.

[8] T. S. Roussy, L. Caldwell, T. Wright, *et al.*, *A new bound on the electron's electric dipole moment*, 2022. arXiv: 2212.11841 [physics.atom-ph].

[9] ACME Collaboration, "Improved limit on the electric dipole moment of the electron," *Nature*, vol. 562, pp. 355–360, 2018. DOI: 10.1038/s41586-018-0599-8.

[10] J. J. Hudson, D. M. Kara, I. J. Smallman, B. E. Sauer, M. R. Tarbutt, and E. A. Hinds, "Improved measurement of the shape of the electron," *Nature*, vol. 473, pp. 493–496, 2011. DOI: 10.1038/nature10104.

[11] A. Boeschoten and L. Willmann, "Perspectives on electric dipole moments of atoms and molecules," *EPJ Web Conf.*, vol. 282, p. 01 019, 2023. DOI: 10.1051/epjconf/202328201019.

[12] P. Aggarwal, H. L. Bethlem, A. Boeschoten, *et al.*, "A supersonic laser ablation beam source with narrow velocity spreads," *Review of Scientific Instruments*, vol. 92, no. 3, p. 033 202, Mar. 2021, ISSN: 0034-6748. DOI: 10.1063/5.0035568.

[13] A. Boeschoten, "Precision measurements in diatomic molecules: a route to a permanent electric dipole moment," Ph.D. dissertation, University of Groningen, 2023. DOI: 10.33612/diss.674231809.

[14] T. B. Meijknecht, "PhD thesis in preparation," *University of Groningen*, 2023.

[15] V. R. Marshall, "PhD thesis in preparation," *University of Groningen*, 2023.

[16] A. Boeschoten, V. R. Marshall, T. B. Meijknecht, *et al.*, *Novel spin-precession method for sensitive EDM searches*, 2023. arXiv: 2303.06402 [physics.atom-ph].

[17] P. Aggarwal, V. R. Marshall, H. L. Bethlem, *et al.*, "Lifetime measurements of the $A\,^2\Pi_{1/2}$ and $A\,^2\Pi_{3/2}$ states in BaF," *Phys. Rev. A*, vol. 100, 5 Nov. 2019. DOI: 10.1103/PhysRevA.100.052503.

[18] Y. Hao, L. F. Pašteka, L. Visscher, *et al.*, "High accuracy theoretical investigations of CaF, SrF, and BaF and implications for laser-cooling," *The Journal of Chemical Physics*, vol. 151, no. 3, p. 034 302, Jul. 2019, ISSN: 0021-9606. DOI: 10.1063/1.5098540.

[19] J. R. Maat, "Calculations on the energy level structure and the effects of external fields in barium monofluoride and the design and construction of an optical trap for nanoparticles as vibration sensors," *University of Groningen*, 2018, Master Thesis.

[20] G. L. Squires, *Practical Physics*, 4th ed. Cambridge University Press, 2001. DOI: 10.1017/CBO9781139164498.

[21] S. A. Self, "Focusing of spherical gaussian beams," *Applied optics*, vol. 22, no. 5, pp. 658–661, 1983.

[22] R. Paschotta, "Gaussian beams," [Online]. Available: https://www.rp-photonics.com/gaussian_beams.html.

[23] Thorlabs, *FiberPort Collimators / Couplers*. [Online]. Available: www.thorlabs.com/newgrouppage9.cfm?objectgroup_id=2940.

[24] O. Böll, Personal communication, Jun. 2023.

[25] T. E. Tiemens, "Investigating the Viability of Using Avalanche Photodiodes for State Detection of BaF in the NL-eEDM Experiment," *University of Groningen*, 2022, Bachelor Thesis.

[26] E. Bobrova Blyumin, "Counting Statistics of an Electron Electric Dipole Moment Experiment," *University of Groningen*, 2023, Bachelor Thesis.

[27] R. Paschotta, "Acousto-optical modulators," [Online]. Available: https://www.rp-photonics.com/acousto_optic_modulators.html.

[28] P. S. Hofstra, "Bachelor thesis in preparation," *University of Groningen*, 2023.

A Code for Simulations

The code written for the simulation method developed as described in Section 3, using Equation 11 is presented here. First, a few different laser intensity distributions are defined, such as the Gaussian and a block wave. This can easily be expanded to account for any mathematically definable distribution. Then, the code for the Lorentzian is presented, as well as the numerical solution to the differential equation. Four graphs are made with different parameters, and are thus presented in the same figure (Figure 7). The benefit of this code structure is that it can be easily expanded if needed, and parameters can be changed quite easily as well.

A.1 Laser Intensity Distributions

```
// writing some inbuilt functions in a simpler way
auto pi = TMath::Pi();

// Defining a few different intensity distributions as functions:

double_t fIofx(double_t *x, double_t *par){
    // Gaussian distribution
    double_t gaussian;
    gaussian = par[0]*exp(-1*pow((x[0]-par[1]),2)/(2*par[2]*par[2]));
    // gaussian = 1;
    return gaussian;
}

double_t gIofx(double_t *x, double_t *par){
    // block wave distribution
    double_t blockwave;
    blockish = par[0]*2*TMath::Floor(x[0])-par[1]*(TMath::Floor(2*x[0]))+par[2];
    return blockwave;
}

// Excitation probability as a function of intensity.
double_t excitation(double_t *x, double_t *par){
    double_t intensity;
    intensity = fIofx(&x[0],&par[3]);
}

// Plotting the function above with a few set parameters
void intensitydistribution(){
    auto gaussian = new TF1("gaussian","fIofx",0,20,3);
    gaussian->SetParameter(0,2);
    gaussian->SetParameter(1,2);
    gaussian->SetParameter(2,1);

    gaussian->Draw();
}
```

A.2 Depletion Function and Excitations

```
   double_t hIofw(double_t *w, double_t *par){
     // Lorentzian distribution with detuning
    double_t lorentzian;
    double_t detune;
```

```
    double_t detune2;
    par[1] = 1/(2*pi*0.057);
    detune = par[0]-w[0];
    detune2 = detune*detune;
    lorentzian = 1/(2*(1+(detune2/par[1])));
    return lorentzian;
}

// Loop to numerically solve the differential equation
double_t loop(double_t *x, double_t *par){
    double_t Nxi;
    double_t intensity;
    double_t prob;
    Nxi = 1;
    double_t f0 = 48;
    double_t f1 = 0;
    double_t z =0;
    double_t zstep = 0.01;

    do{
        intensity = fIofx(&z,&par[0]);
        prob = hIofw(&par[4],&f1);
        Nxi -= Nxi*zstep*intensity*prob;
        z+=zstep;
    }while(z<x[0]);
    return Nxi;
}

// Graphing the various results
void depletionfunction(double_t detuning = 5, double_t Intensity = 5){

    // Depletion function with detuning
    auto detuned = new TF1("detuned","loop",36,40,5);
    detuned->SetParameter(0,Intensity);
    detuned->SetParameter(1,38.4);
    detuned->SetParameter(2,0.5);
    detuned->SetParameter(3,1);
    detuned->SetParameter(4,detuning);
    detuned->SetTitle("Intensity = 5mW, Detuning = 5MHz");
    detuned->SetLineColor(2);

    cout << detuned->Eval(50) << endl;

    // Depletion function with "standard" intensity and no detuning
    auto standard = new TF1("standard","loop",36,40,5);
    standard->SetParameter(0,5);
    standard->SetParameter(1,38.4);
    standard->SetParameter(2,0.5);
    standard->SetParameter(3,1);
    standard->SetParameter(4,0);
    standard->SetTitle("Intensity = 5mW, Detuning = 0MHz");

    cout << standard->Eval(50) << endl;

    // Depletion function with intensity set to be very small
    auto undersaturated = new TF1("undersaturated","loop",36,40,5);
    undersaturated->SetParameter(0,0.1);
```

```
    undersaturated->SetParameter(1,38.4);
    undersaturated->SetParameter(2,0.5);
    undersaturated->SetParameter(3,1);
    undersaturated->SetParameter(4,0);
    undersaturated->SetTitle("Intensity = 0.1mW, Detuning = 0MHz");
    undersaturated->SetLineColor(8);

    cout << undersaturated->Eval(50) << endl;

    // Depletion function with intensity set to be very high
    auto oversaturated = new TF1("oversaturated","loop",36,40,5);
    oversaturated->SetParameter(0,50);
    oversaturated->SetParameter(1,38.4);
    oversaturated->SetParameter(2,0.5);
    oversaturated->SetParameter(3,1);
    oversaturated->SetParameter(4,0);
    oversaturated->SetTitle("Intensity = 50mW, Detuning = 0MHz");
    oversaturated->SetLineColor(4);

    cout << oversaturated->Eval(50) << endl;

    // Making the graphs individually
    auto gr1 = new TGraph(detuned);
    auto gr2 = new TGraph(standard);
    auto gr3 = new TGraph(undersaturated);
    auto gr4 = new TGraph(oversaturated);

    // Adding all the above graphs to the same figure
    auto gr = new TMultiGraph();
    gr->Add(gr2);
    gr->Add(gr3);
    gr->Add(gr4);
    gr->Add(gr1);

    // Setting some standard styles for the whole figure
    gr->SetTitle("Depletion Function; Position z(t) [10^{-1}m]; Probability(F=1)
    ");
    gr->GetYaxis()->SetNdivisions(1010);
    gr->GetYaxis()->SetRangeUser(0,1.1);
    gr->GetXaxis()->SetNdivisions(1010);
    gr->Draw("AWL");
    // command below only works once the canvas has already been made
    c1->BuildLegend();
}
```